SUPPLEMENTARY INFORMATION

Ongoing intensification of El Niño impacts on East Asia's summer climate with achieved carbon neutrality

Wen Zhang[1,3,5], Weichen Tao[1,5*], Gang Huang[1,2,3*], Kaiming Hu[1,4], Xia Qu[1,4], Ya Wang[1], Haosu Tang[1], and Suqin Zhang[1,3]

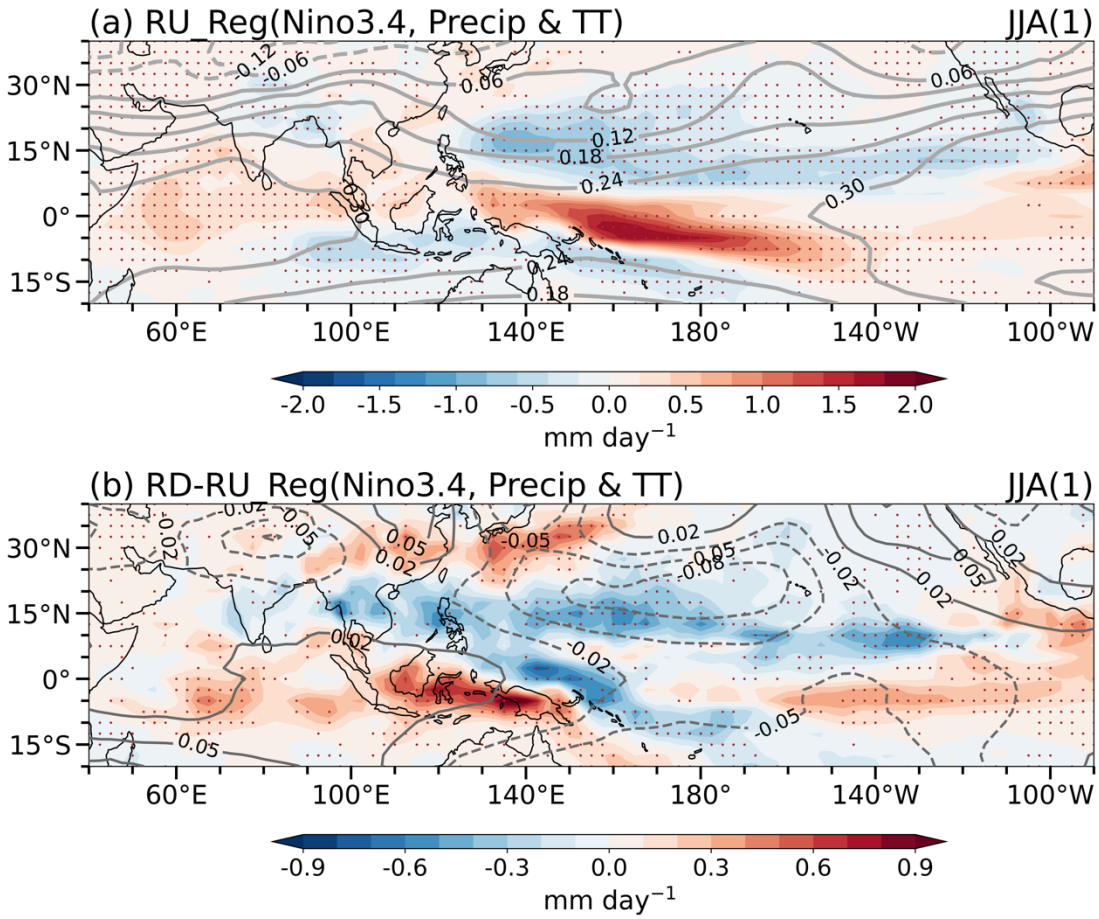

Supplementary Figure 1. The spatial field of the precipitation anomalies and air temperature anomalies. (a) Regressed precipitation anomalies (shading; unit: mm day^{-1}) and vertically averaged (850-200 hPa) air temperature anomalies (contours; unit: °C) during JJA(1) onto the D(0)JF(1) Niño-3.4 index in the CO_2 RU period for 9 models' MME. (b) Same as (a), but for the differences between the CO_2 RD and RU period. Brown dots denote that at least 70% models show consistent results.

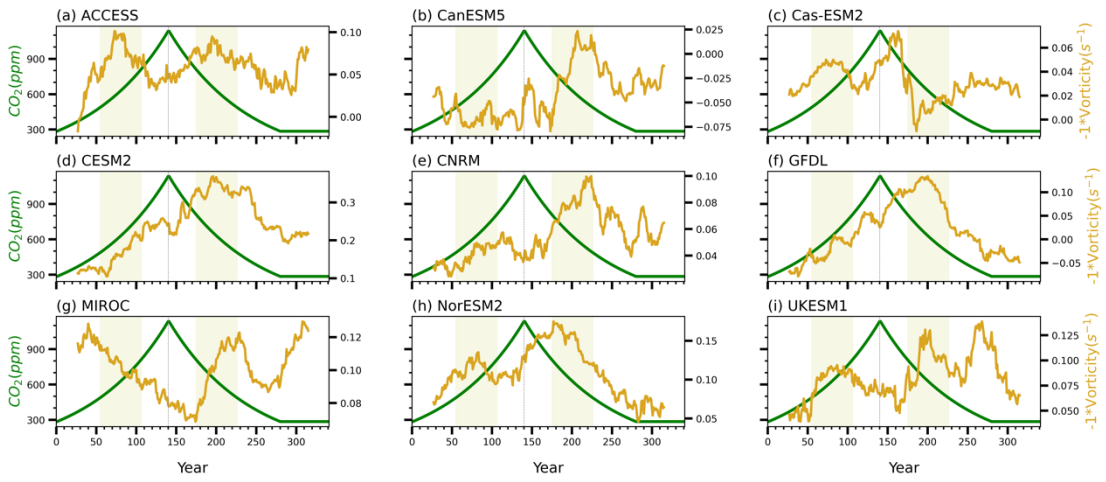

Supplementary Figure 2. Same as Fig. 1b, but for the evolution of CO_2 concentrations and WNPAC intensity in each model.

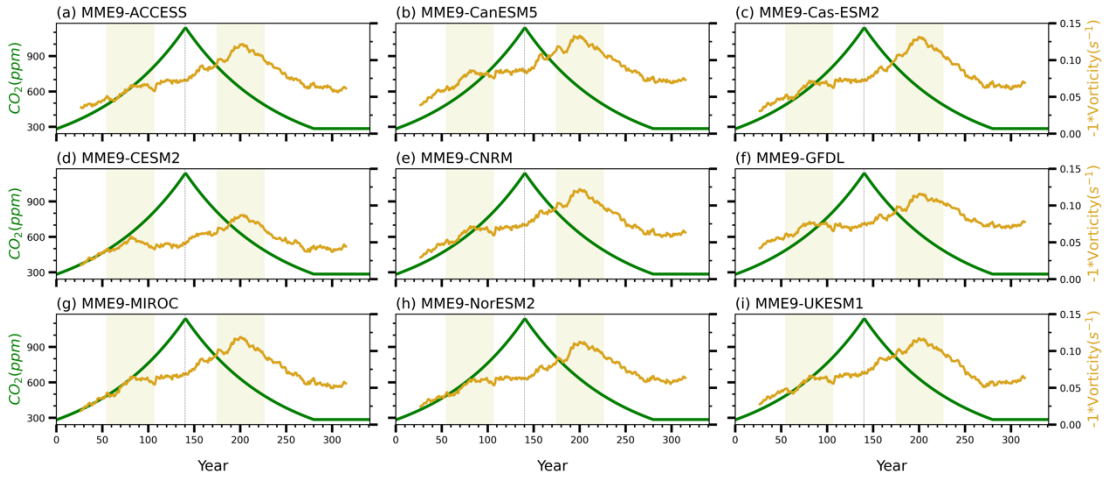

Supplementary Figure 3. Same as Fig. 1b, but for evolution of CO_2 concentrations and WNPAC intensity for 8 models' MME after excluding individual models.

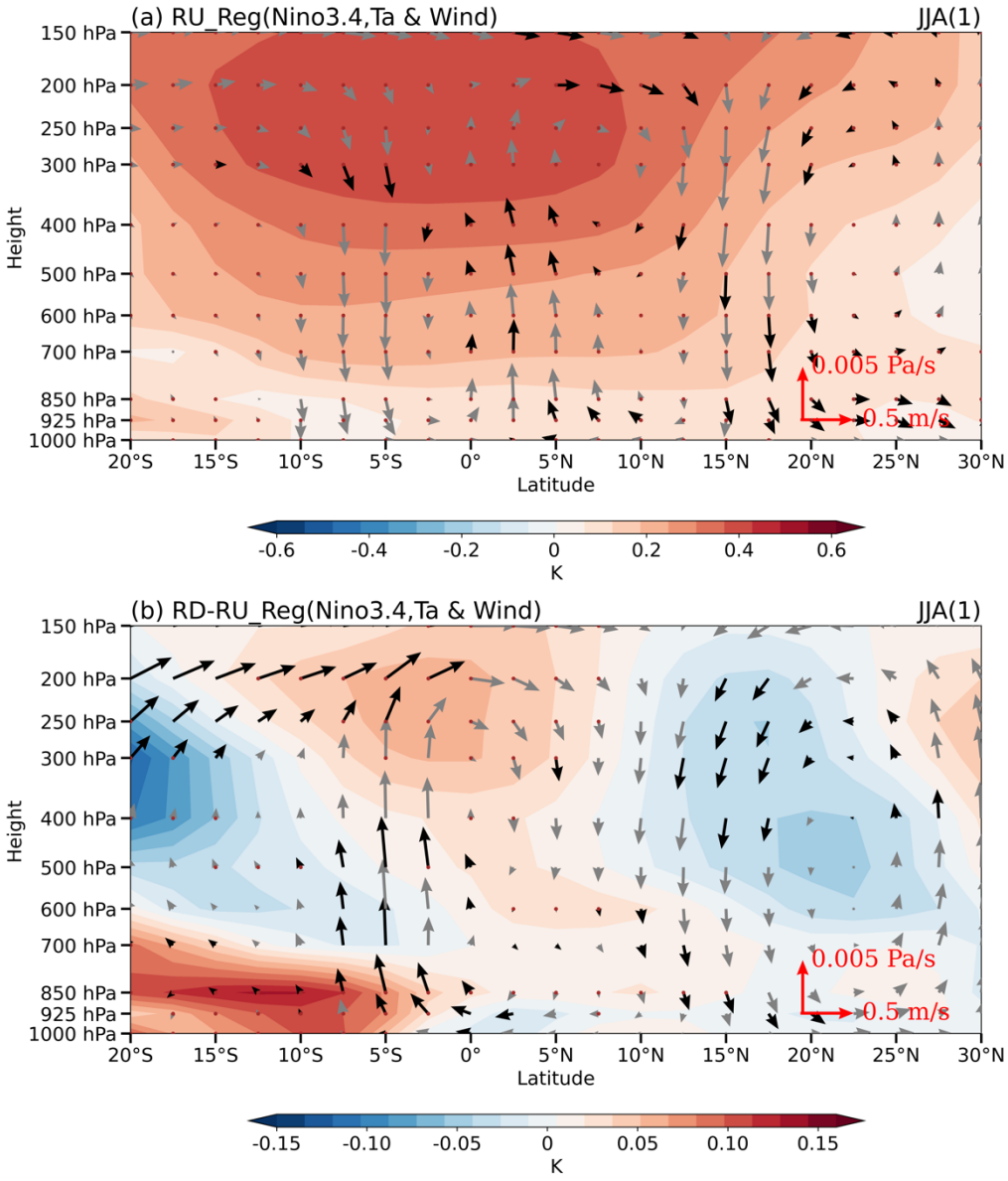

Supplementary Figure 4. Meridional circulation anomalies and atmospheric temperature anomalies. (a) Regressed zonal mean atmospheric temperature anomalies (shading; unit: K) and wind anomalies (arrows; units: Pa s^{-1} and m s^{-1}) from 65°E to 105°E during JJA(1) onto the D(0)JF(1) Niño-3.4 index in the CO_2 RU period for 9 models' MME. (b) Same as (a), but for the differences between the CO_2 RD and RU period. The black arrows and brown dots denote that at least 70% models show consistent results.

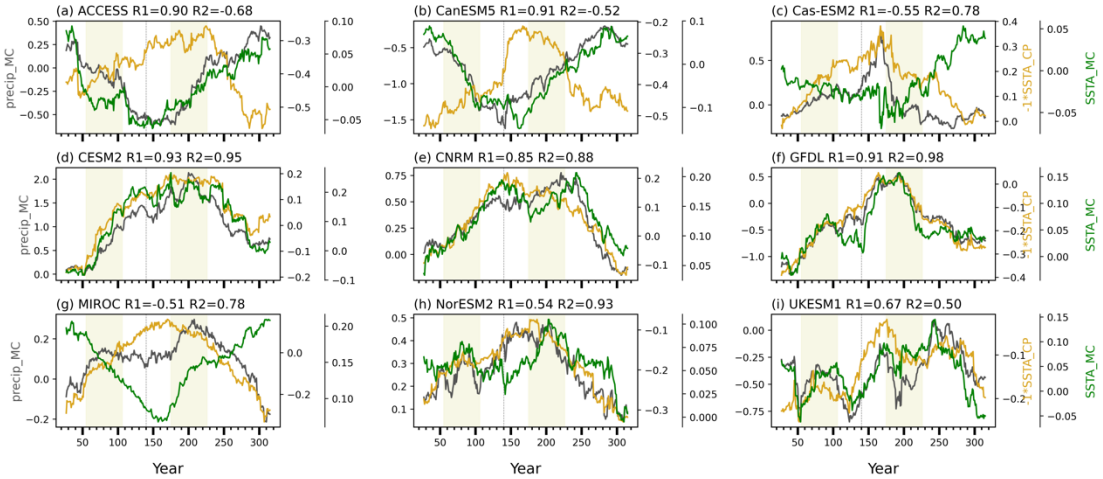

Supplementary Figure 5. Evoution of SST anomalies in the MC, SST anomalies in the equatorial CP, and precipitation anomalies in the MC. Regressed precipitation anomalies in the MC (grey line; unit: mm day^{-1}), SST anomalies in the CP (yellow line; unit: K), and SST anomalies in the MC (green line; unit: K) during JJA(1) onto the D(0)JF(1) Niño-3.4 index in each model. R1 and R2 in the title respectively denote the correlation coefficients between the SST anomalies and precipitation anomalies in the MC, and between the SST anomalies in the equatorial CP and precipitation anomalies in the MC. The green shadings and dashed vertical lines are same as in Fig. 1b.

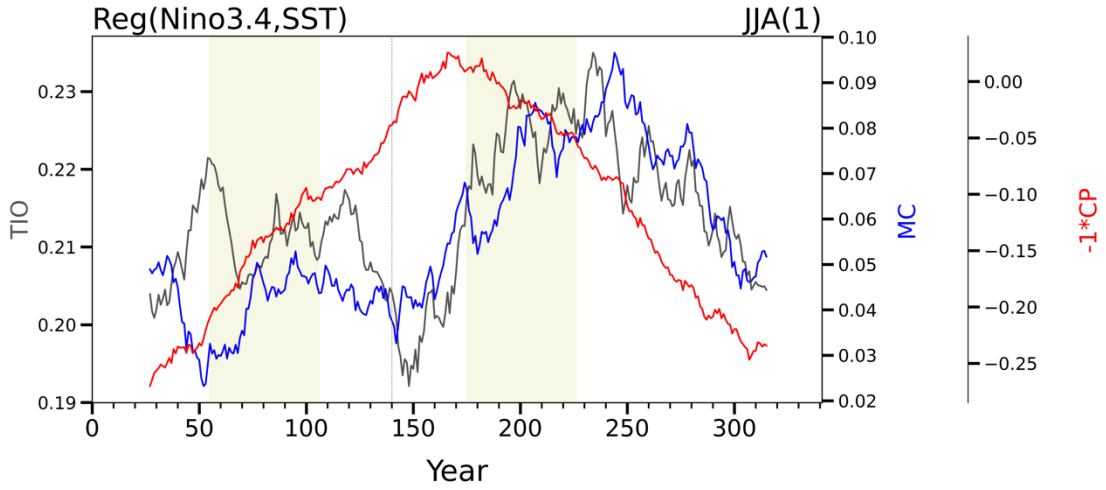

Supplementary Figure 6. Evolution of SST anomalies in the TIO, MC and equatorial CP. Regressed the SST anomalies in the TIO (grey line; unit: K), MC (blue line; unit: K), and equatorial CP (red line; unit: K) during JJA(1) onto the D(0)JF(1) Niño-3.4 index for 9 models' MME. The green shadings and dashed vertical lines are same as in Fig. 1b.

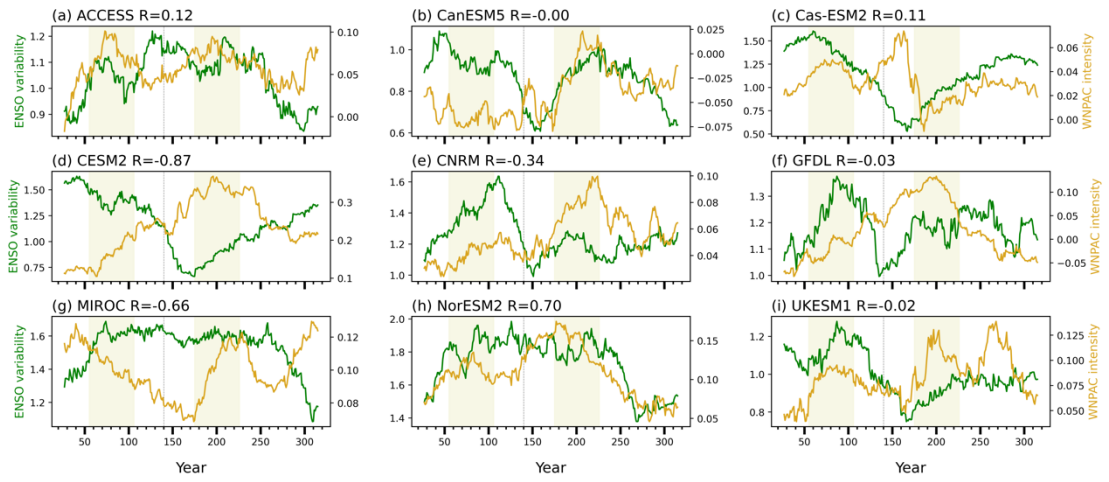

Supplementary Figure 7. Evolution of ENSO variability and the WNPAC intensity. The standard deviation of D(0)JF(1) Niño 3.4 index and the WNPAC intensity during JJA(1) in each model. The R in the title denotes the correlation coefficient between them two. The green shadings and dashed vertical lines are same as in Fig. 1b.

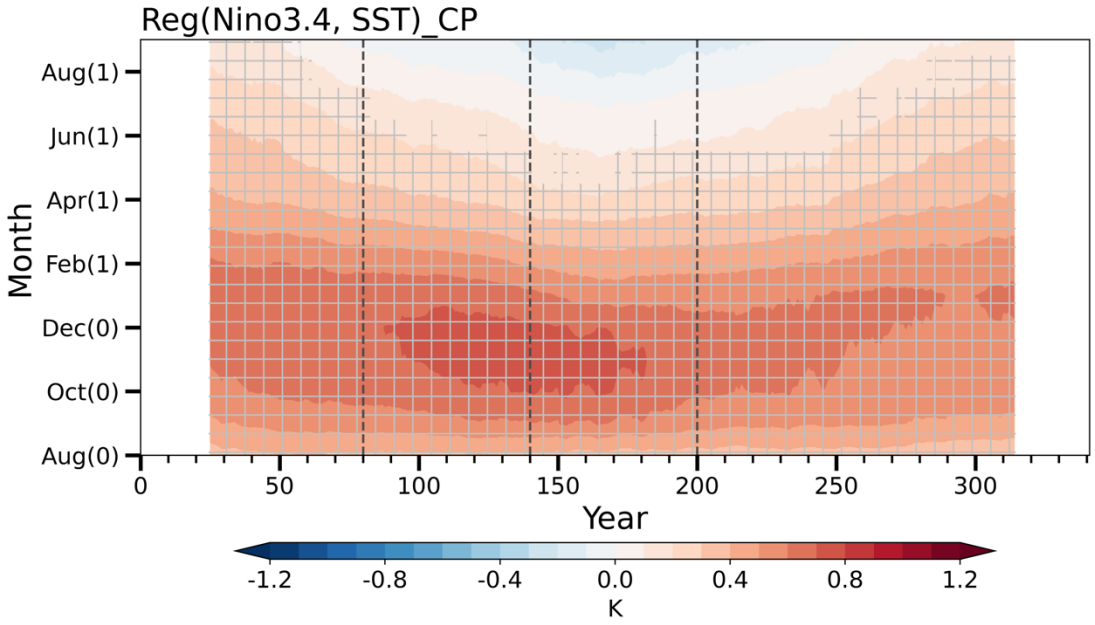

Supplementary Figure 8. Changes of SST anomalies in the equatorial CP. Hovmöller diagrams of regressed SST anomalies (unit: K) in the equatorial CP (7.5°S-7.5°N, 160°E-160°W) onto the D(0)JF(1) Niño-3.4 index for 5 models' MME. Gray grids and the vertical dashed lines are same as in Fig. 2a.

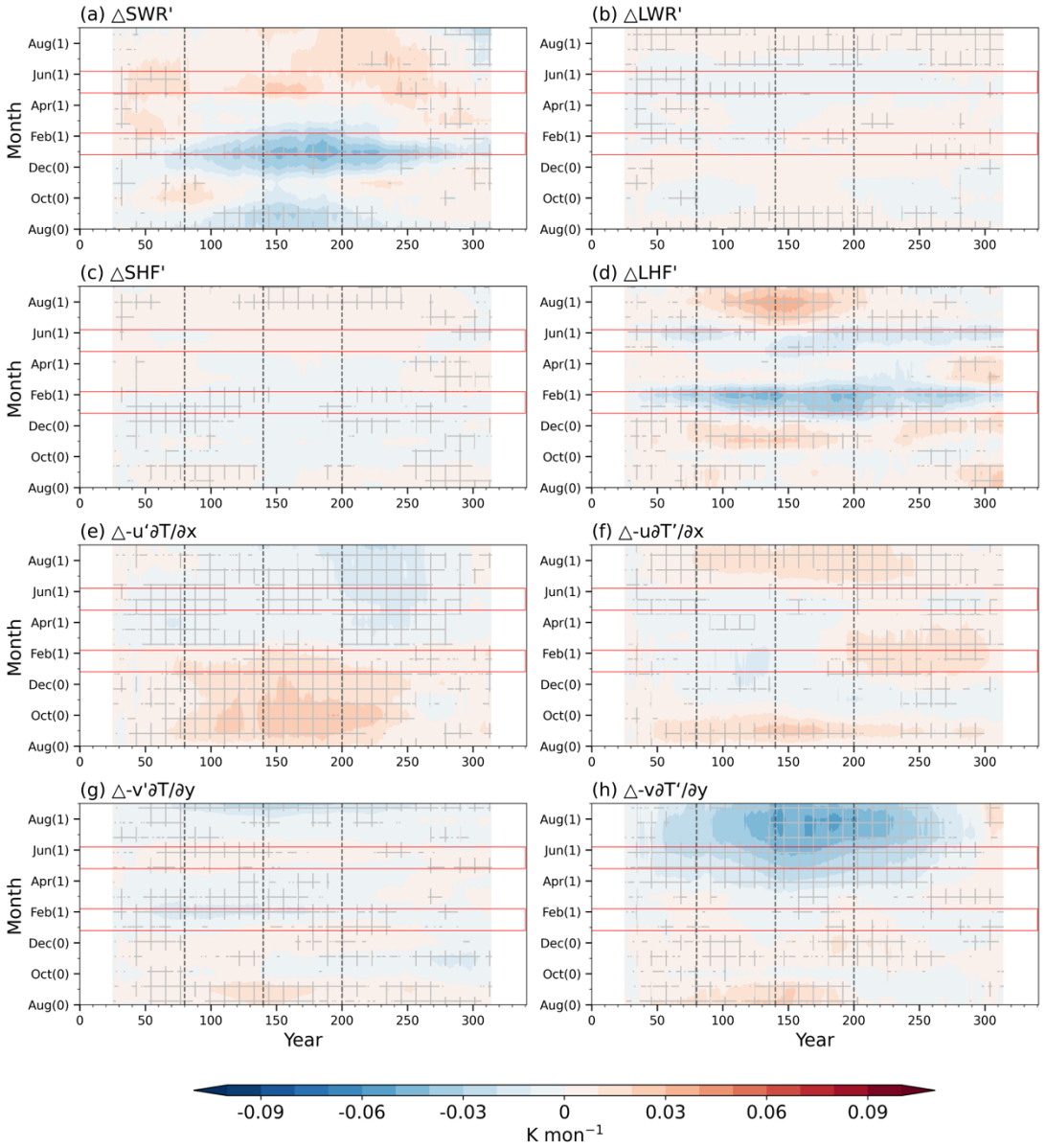

Supplementary Figure 9. Contributions of each term from the mixed-layer temperature budget in the equatorial CP. Hovmöller diagrams of (a) the SWR anomalies (units: K month^{-1}), (b) the LWR anomalies (units: K month^{-1}), (c) the SHF anomalies (units: K month^{-1}), (d) the LHF anomalies (units: K month^{-1}), (e) the anomalous zonal advection of the mean potential temperature gradient ($-u' \partial \bar{T}/\partial x$; units: K month^{-1}), (f) the mean zonal advection of the anomalous potential temperature gradient ($-\bar{u}\, \partial T'/\partial x$; units: K month^{-1}), (g) the anomalous meridional advection of the mean

potential temperature gradient ($-v'\,\partial\bar{T}/\partial y$; units: K month^{-1}), and (h) the mean meridional advection of anomalous temperature gradient ($-\bar{v}\,\partial T'/\partial y$; units: K month^{-1}) for 5 models' MME. The red solid line rectangles, gray grids, dashed vertical lines, prime symbols, and Δ symbols are same as in Fig. 2a.

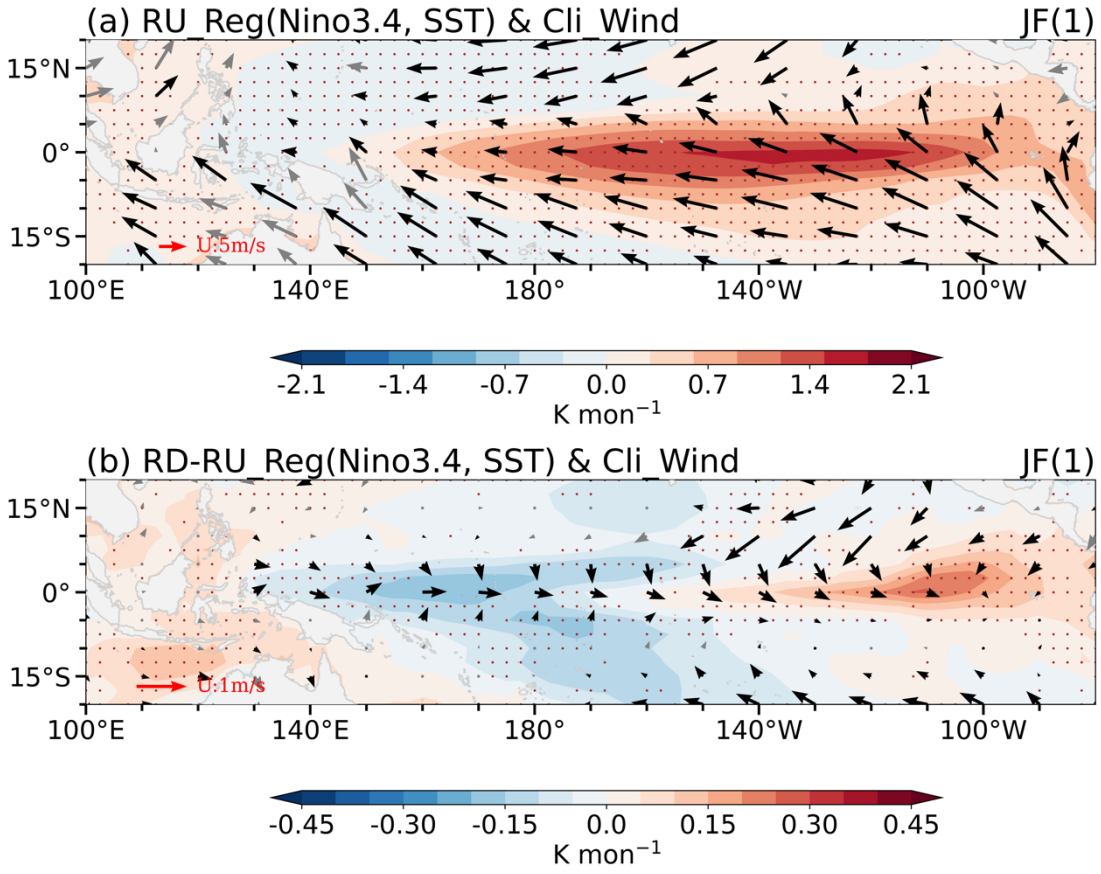

Supplementary Figure 10. The spatial field of the mean winds and SST anomalies. (a) Regressed SST anomalies (shading; unit: K) during JF(1) onto the D(0)JF(1) Niño-3.4 index and 1000-hPa climatological mean winds (vectors; unit: m s^{-1}) in the CO_2 RU period for 5 models' MME. (b) Same as (a), but for the differences between the CO_2 RD and RU period. The black arrows and brown dots denote that at least 70% models show consistent results.

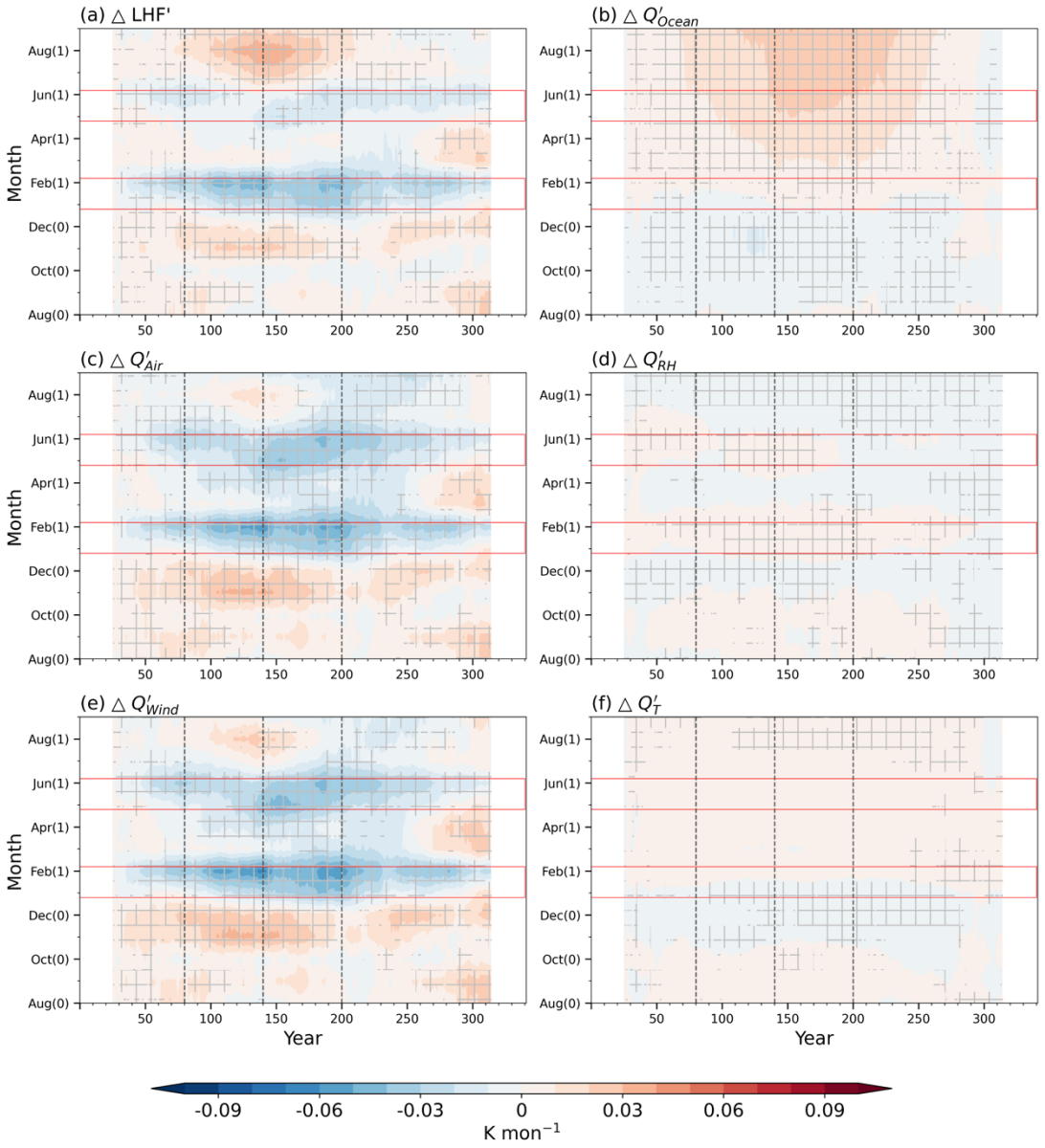

Supplementary Figure 11. The components of LHF anomalies in the equatorial CP. Hovmöller diagrams of (a) the LHF anomalies (units: K month^{-1}), (b) the LHF anomalies induced by oceanic responses (units: K month^{-1}), (c) the LHF anomalies induced by atmospheric forcing (units: K month^{-1}), (d) the LHF anomalies induced by relative humidity (units: K month^{-1}), (e) the LHF anomalies induced by wind (units: K month^{-1}), and (f) the LHF anomalies induced by sea-air temperature difference (units:

K month^{-1}) for 5 models' MME. The red solid line rectangles, gray grids, dashed vertical lines, prime symbols, and Δ symbols are same as in Fig. 2a.

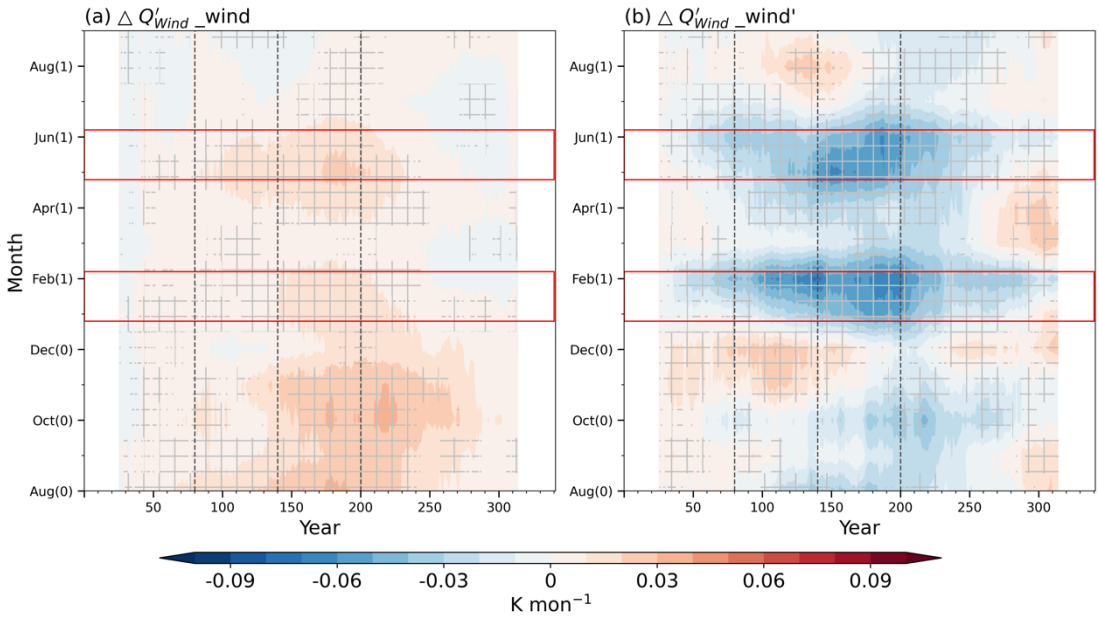

Supplementary Figure 12. The decomposition of wind-induced LHF anomalies in the equatorial CP. (a) Hovmöller diagram of the wind-induced LHF anomalies due to the climatological mean wind (units: K month^{-1}) in the equatorial CP for 5 models' MME. (b) Same as (a), but the effects of wind anomalies. The red solid line rectangles, gray grids, dashed vertical lines, prime symbols, and Δ symbols are same as in Fig. 2a.

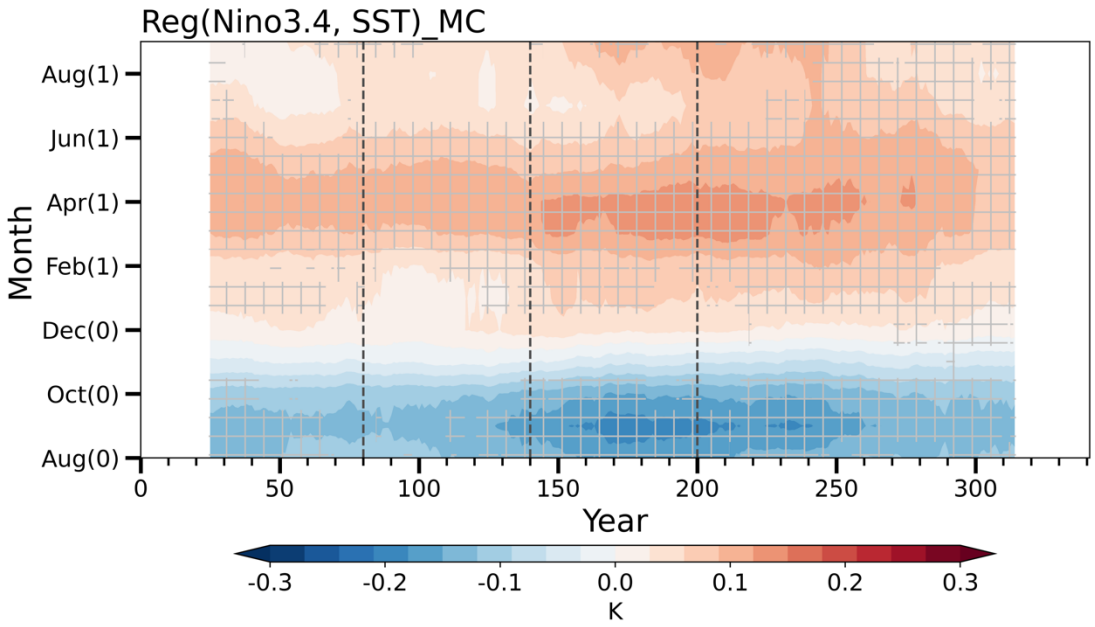

Supplementary Figure 13. As in Supplementary Fig. 8, but for the MC.

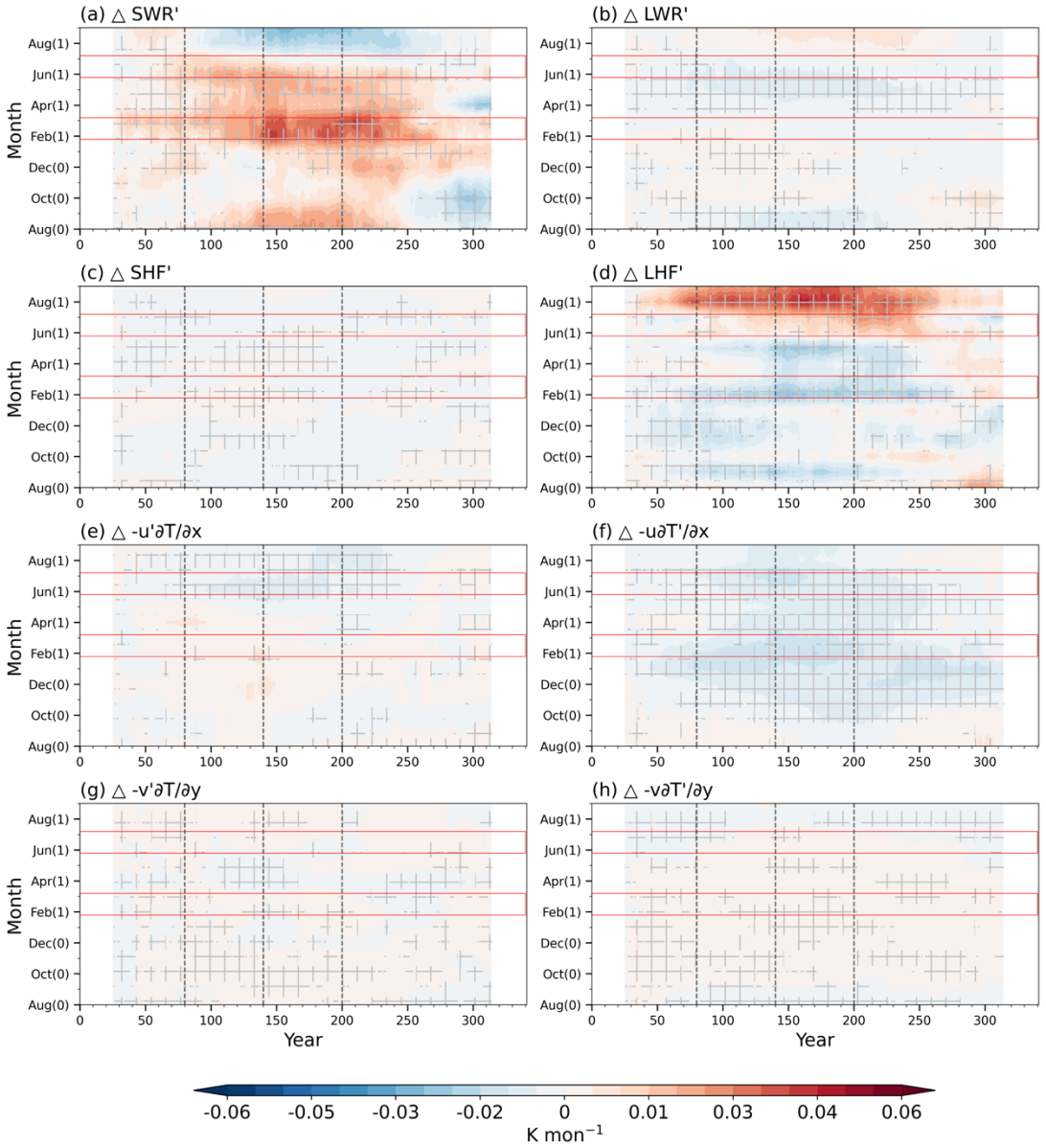

Supplementary Figure 14. As in Supplementary Fig. 9, but for the MC.

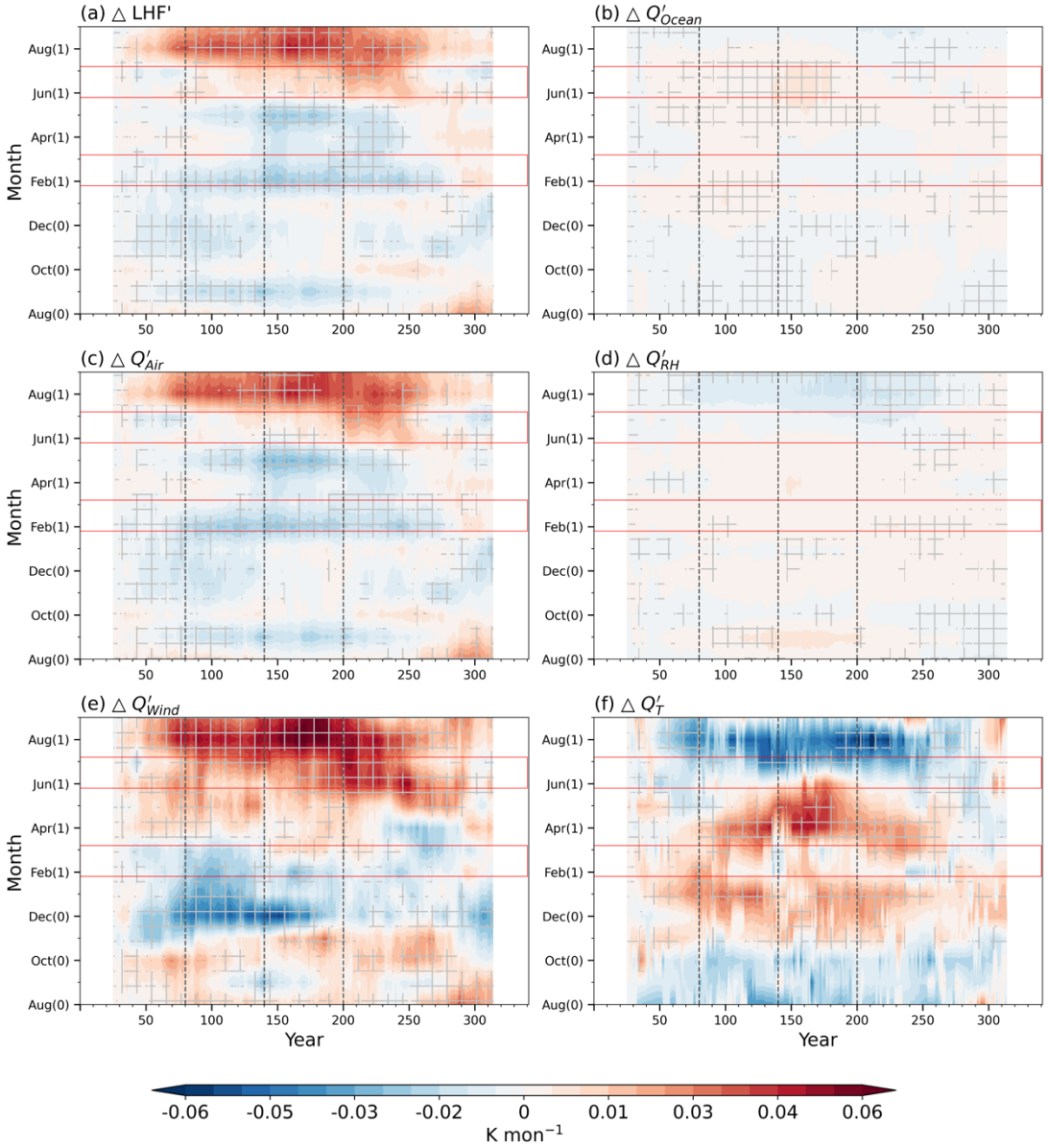

Supplementary Figure 15. As in Supplementary Fig. 11, but for the MC.

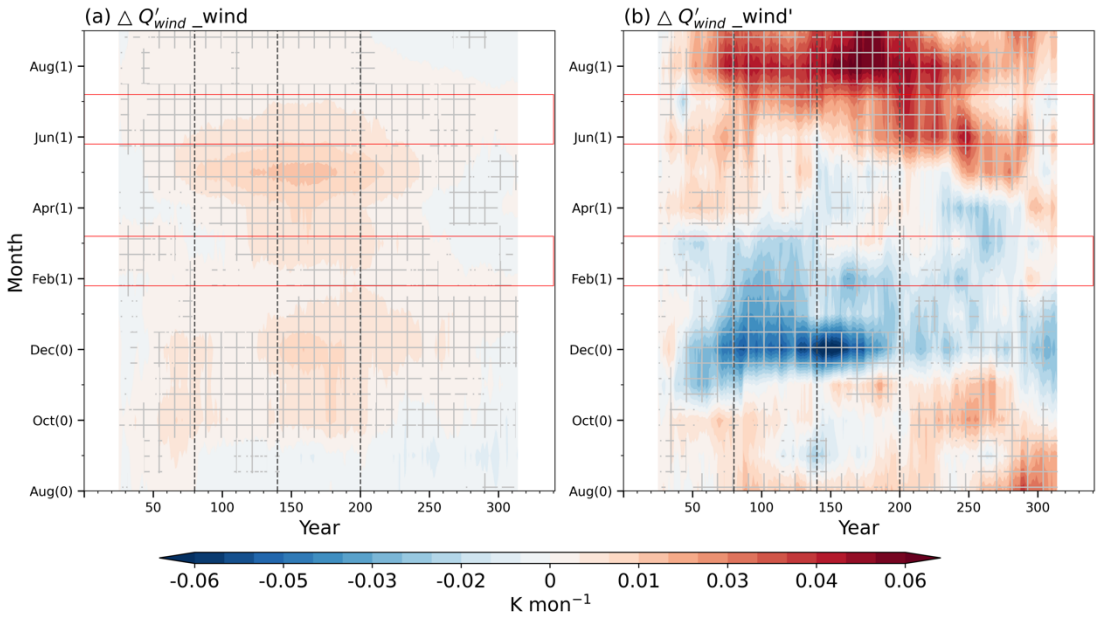

Supplementary Figure 16. As in Supplementary Fig. 12, but for the MC.

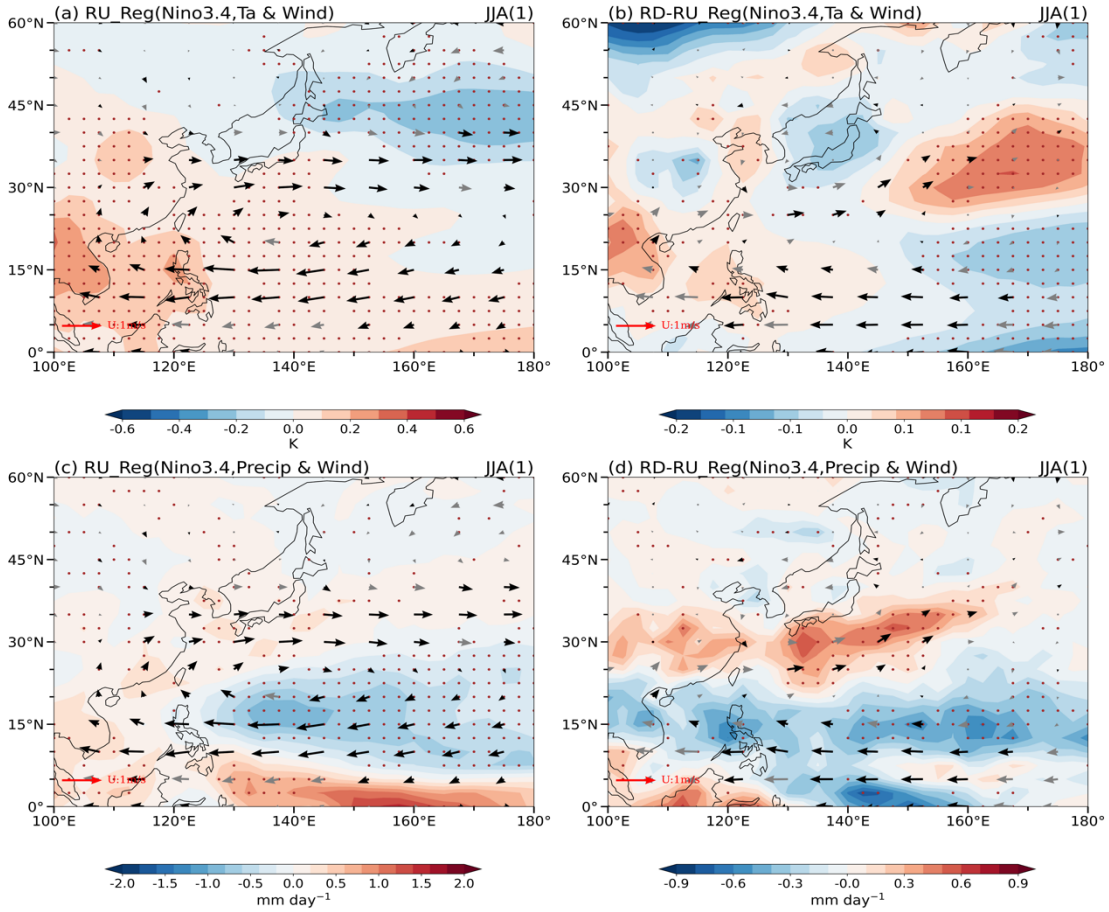

Supplementary Figure 17. The spatial field of the surface air temperature anomalies and precipitation anomalies. (a**)** Regressed surface air temperature anomalies (shading; unit: K) and 850-hPa wind anomalies (vectors; unit: m s^{-1}) during JJA(1) onto the D(0)JF(1) Niño-3.4 index in the CO_2 RU period for 9 models' MME. (b**)** Same as (a), but for the differences between the CO_2 RD and RU period. (c**)** Regressed precipitation anomalies (shading; unit: mm day^{-1}) and 850-hPa wind anomalies (vectors; unit: m s^{-1}) during JJA(1) onto the D(0)JF(1) Niño-3.4 index in the CO_2 RU period for 9 models' MME. (d) Same as (c), but for the differences between the CO_2 RD and RU period. The black arrows and brown dots denote that at least 70% models show consistent results.

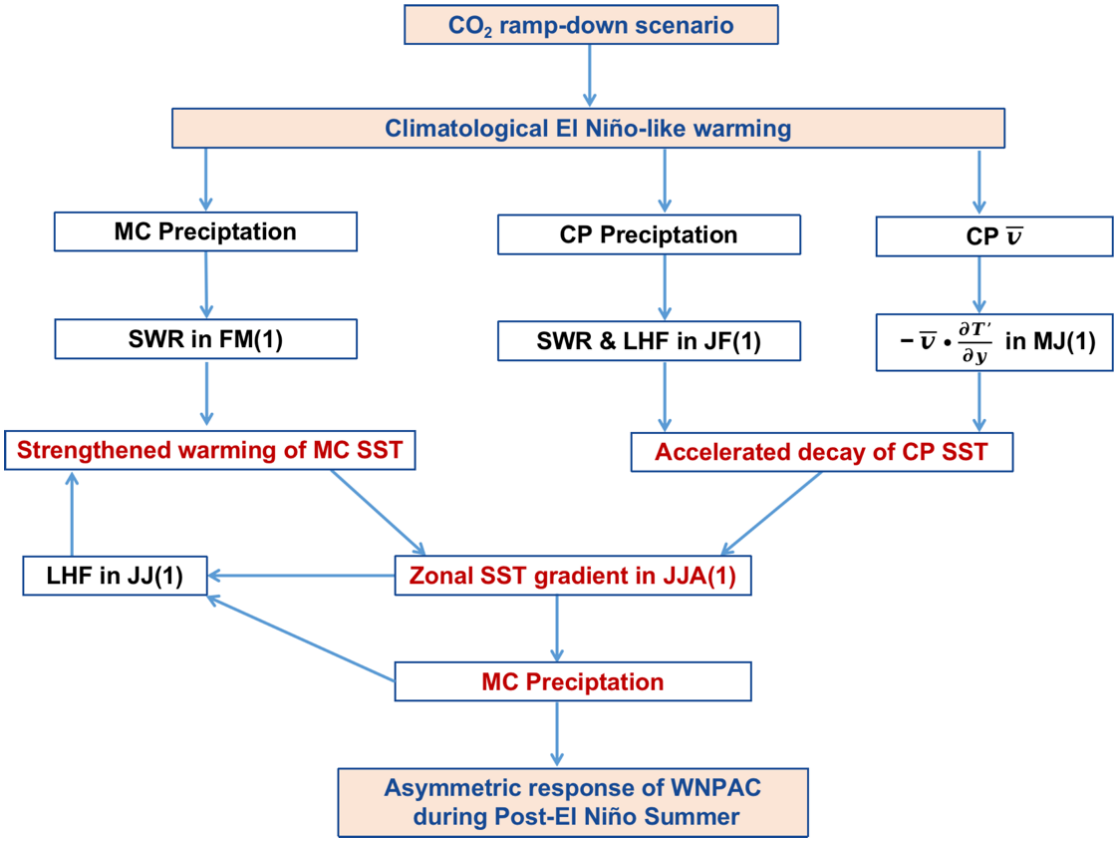

Supplementary Figure 18. Key processes involved in the asymmetric response of the anomalous WNPAC intensity during post-El Niño summer.